Supporting Information

WS_2/Polyethylene Glycol Nanostructures for Ultra-Efficient MCF-7 Cancer Cell Ablation and Electrothermal Therapy

Maria Prisca Meivita,[1] Sophia S. Y. Chan,[1] Shao Xiang Go,[1] Denise Lee,[1] Natasa Bajalovic,[1,*] Desmond K. Loke[1,2,*]

[1]*Department of Science, Mathematics and Technology, Singapore University of Technology and Design, Singapore 487372, Singapore*

[2]*Office of Innovation, Changi General Hospital, Singapore, 529889, Singapore*

[*]*Correspondence and requests for materials should be addressed to N.B. (email: natasa_bajalovic@sutd.edu.sg) or D.K.L. (email: desmond_loke@sutd.edu.sg)*

Table S1. Thermoelectric properties of the cell-layer/nanostructure model utilized in electrothermal simulations.

Material	Isotropic thermal conductivity (W/mK)	Isotropic resistivity (Ω cm)
SiO_2	1.4	10^{16}
ITO	4	0.0001
PEG	0.285	104
DMEM	0.6667	59.52
Cell	0.6	136
WS_2	140	1.52

Table S2. Statistical significance analysis of MCF-7 and MCF-10A cytotoxicity at different concentrations (0 – 100 μM) of (a) pure WS_2 and (b) WS_2/PEG compared to control (cells only) and within two cell lines. Significance was set based on the Student's t-test and indicated as: * ($p < 0.05$), ** ($p < 0.01$), *** ($p < 0.001$), **** ($p < 0.0001$). Non-significant results were unmarked.

(a) WS_2		**Concentrations (μM)**			
		25	**50**	**75**	**100**
MCF-7	relative to control		****	****	****
MCF-10A	relative to control				*
MCF-7	relative to MCF-10A		*	**	**

(b) WS_2/PEG		**Concentrations (μM)**			
		25	**50**	**75**	**100**
MCF-7	relative to control				*
MCF-10A	relative to control				
MCF-7	relative to MCF-10A				

Table S3. References for Figure 4d.

Ref No.	Reference	Energy density (J/ml)	Electric field (kV/cm)
1	Kumar, G.; Shelar, S.; Patel, A.; Roy, A.; Sarathi, R.; Singh, R.; Sharma, A. Investigation of Effect of Nanosecond Pulsed Electric Field on MCF-7 Breast Cancer Cells. *J. Drug Deliv. Ther.* **2021**, *11* (3), 43–49. DOI: 10.22270/jddt.v11i3.4827.	12.75	18
2	Nuccitelli, R.; McDaniel, A.; Anand, S.; Cha, J.; Mallon, Z.; Berridge, J. C.; Uecker, D. Nano-Pulse Stimulation Is a Physical Modality That Can Trigger Immunogenic Tumor Cell Death. *J. Immunother. Cancer* **2017**, *5* (1), 32. DOI: 10.1186/s40425-017-0234-5.	5	12

Table S4. References for Figure S5.

Ref No.	Reference	Type of nanostructure
1	Guan, G.; Wang, X.; Li, B.; Zhang, W.; Cui, Z.; Lu, X.; Zou, R.; Hu, J. "Transformed" Fe 3 S 4 Tetragonal Nanosheets: A High-Efficiency and Body-Clearable Agent for Magnetic Resonance Imaging Guided Photothermal and Chemodynamic Synergistic Therapy. *Nanoscale* **2018**, *10* (37), 17902–17911. DOI: 10.1039/C8NR06507A.	Fe_3S_4/PVP
2	Hao, J.; Song, G.; Liu, T.; Yi, X.; Yang, K.; Cheng, L.; Liu, Z. In Vivo Long-Term Biodistribution, Excretion, and Toxicology of PEGylated Transition-Metal Dichalcogenides MS2 (M = Mo, W, Ti) Nanosheets. *Adv. Sci.* **2016**, *4* (1), 1600160. DOI: 10.1002/advs.201600160.	MoS_2/PEG

Table S5. References for Figure S7.

Ref No.	Reference
1	Burford, C. D.; Bhattacharyya, K. D.; Boriraksantikul, N.; Whiteside, P. J. D.; Robertson, B. P.; Peth, S. M.; Islam, N. E.; Viator, J. A. Nanoparticle Mediated Thermal Ablation of Breast Cancer Cells Using a Nanosecond Pulsed Electric Field. *IEEE Trans. NanoBioscience* **2013**, *12* (2), 112–118. DOI: 10.1109/TNB.2013.2257836.
2	Mi, Y.; Li, P.; Liu, Q.; Xu, J.; Yang, Q.; Tang, J. Multi-Parametric Study of the Viability of in Vitro Skin Cancer Cells Exposed to Nanosecond Pulsed Electric Fields Combined With Multi-Walled Carbon Nanotubes. *Technol. Cancer Res. Treat.* **2019**, *18*, 1533033819876918. DOI: 10.1177/1533033819876918.

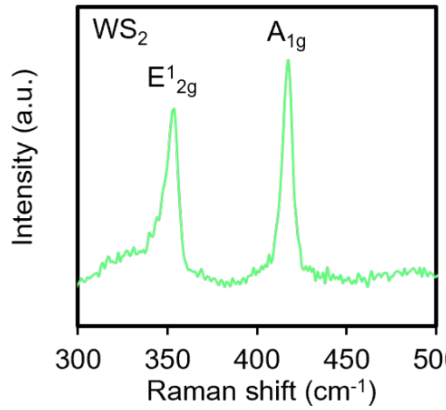

Figure S1. Raman spectra of pure WS_2.

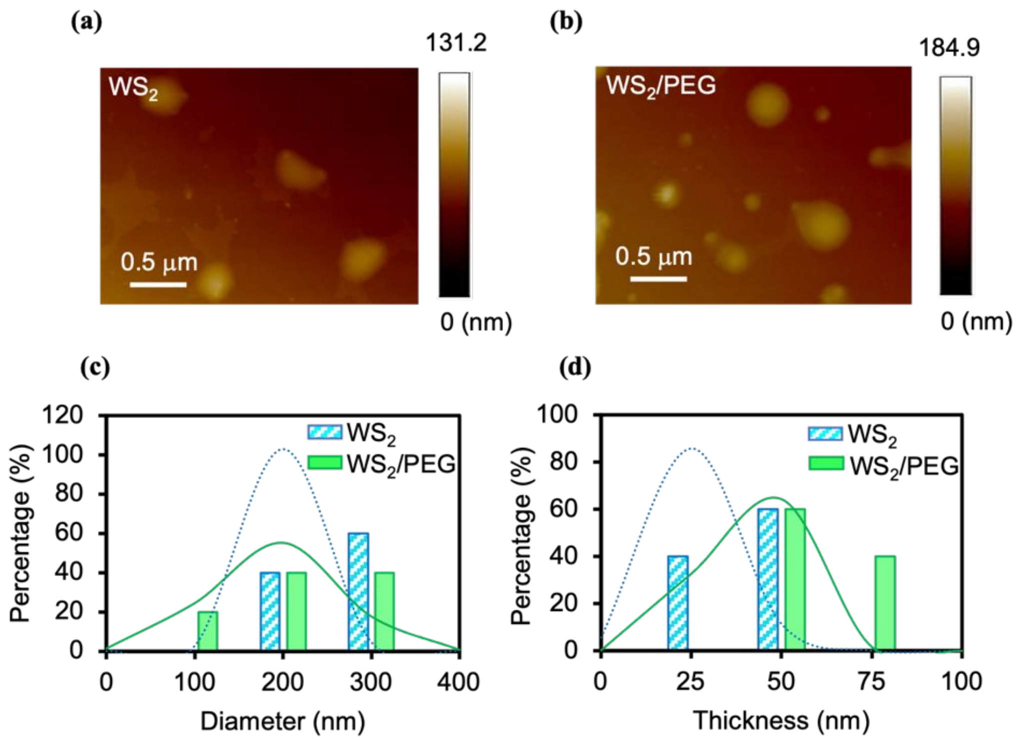

Figure S2. a, b) AFM images of a) pure WS_2 and b) WS_2/PEG nanostructures. **c, d)** Diameter and thickness distributions of c) pure WS_2 and d) WS_2/PEG nanostructures. The data were obtained from a, b).

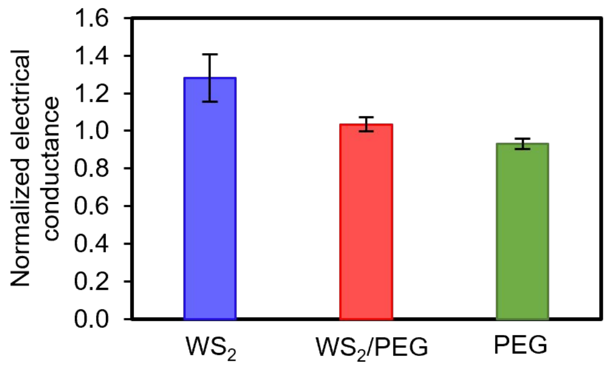

Figure S3. Conductance of pure WS_2, WS_2/PEG and PEG measured in DMEM (MCF-7 cell media). The values were normalized to DMEM conductance, and the error bars represent SEM from 3 independent experiments (n = 3).

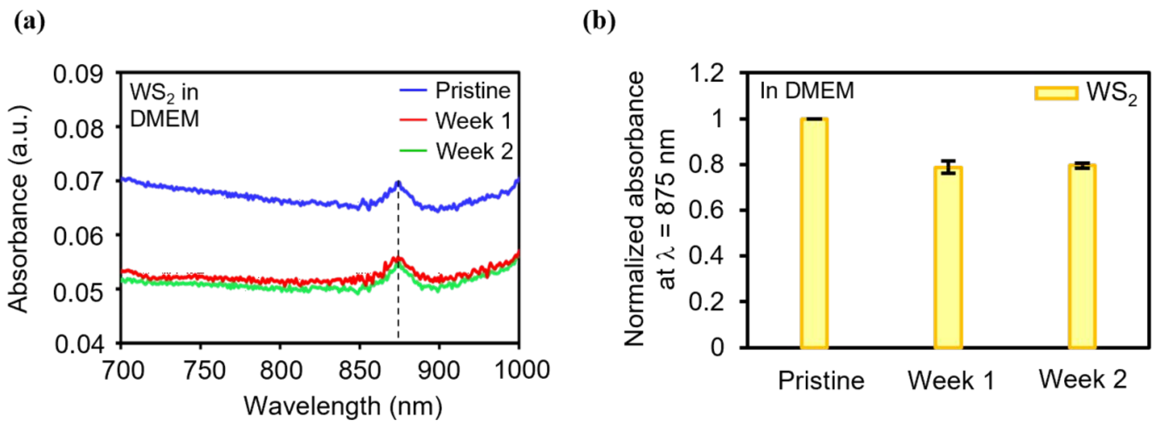

Figure S4. a) Absorbance spectra of pure WS_2 stored in DMEM for different weeks. **b)** Variation of the normalized absorbance at λ = 875 nm for pure WS_2 stored in DMEM in different weeks.

Absorbance spectra with a similar behavior have been demonstrated by the pure transition metal dichalcogenide (TMD-) and TMD/PEG-based nanostructures utilized by other research groups (the absorbance spectra of TMD exhibit a strong absorbance, which was not affected by the PEG modification).[1–3] The nanostructures used in this work show a similar set of curves, which indicates that our results are similar.

The TMD/ BP nanostructures utilized by other research groups demonstrate absorbance spectra with a decrease in absorbance due to degradation.[4–6] A similar set of absorbance curves were obtained for the nanostructures used in this work, indicating that our studies disclose similar results.

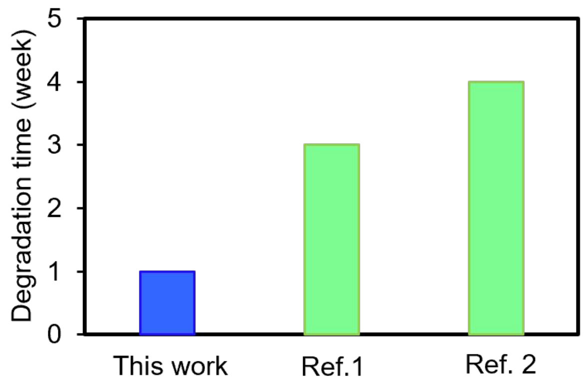

Figure S5. Comparison of the degradation time of WS_2 with that of current nanostructure-based systems in physiological media. The information of the references can be found in Table S4.

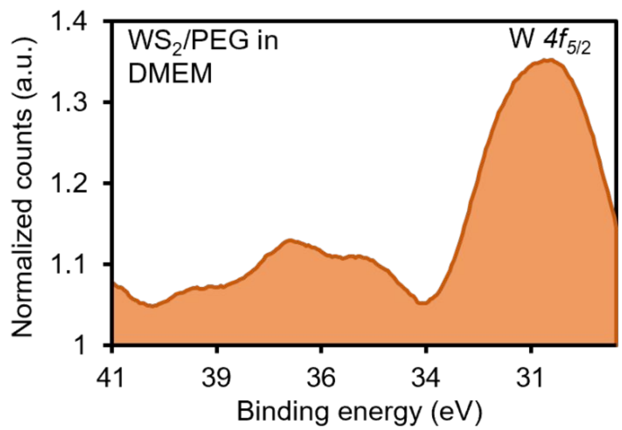

Figure S6. XPS spectra showing the binding energies of W $4f_{7/2}$ of the WS_2/PEG stored in DMEM for a week. The XPS counts were normalized to background.

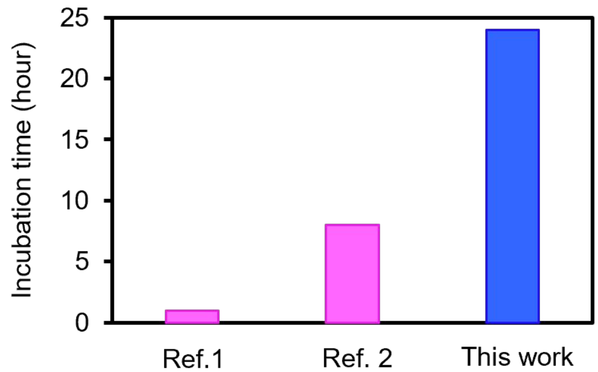

Figure S7. Comparison of the incubation time of WS_2/PEG nanostructures with that of current thermal-based therapeutic methods and with the use of the time of incubation of nanostructures in cells before application of a stimulus as a measure of incubation time. The information of the references can be found in Table S5.

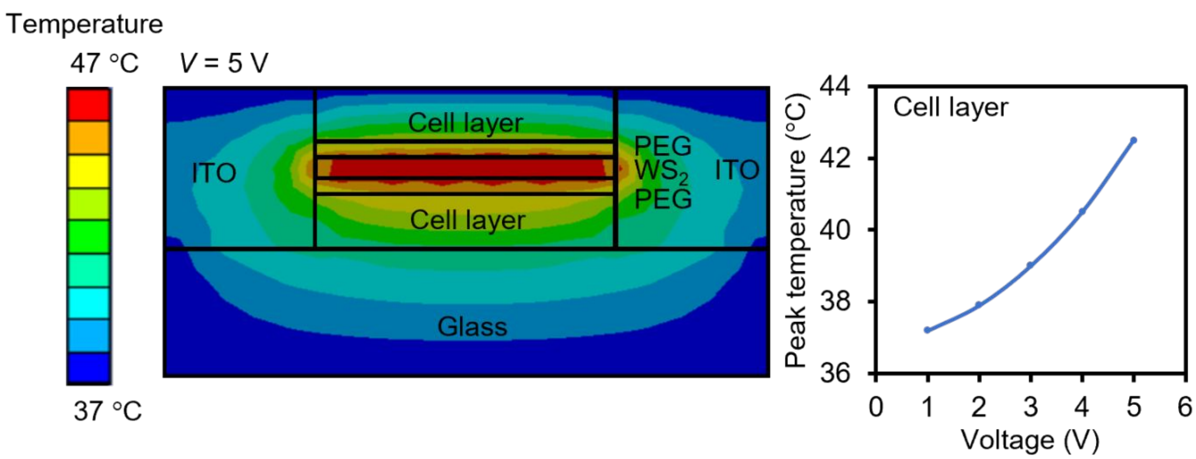

Figure S8. Thermal distribution of a cell-layer/nanostructure model. WS_2/PEG was inserted in the middle of the cell layer, and a square-wave single-pulse was applied. The cell and material structures were constructed on an ITO-on-glass subsystem.

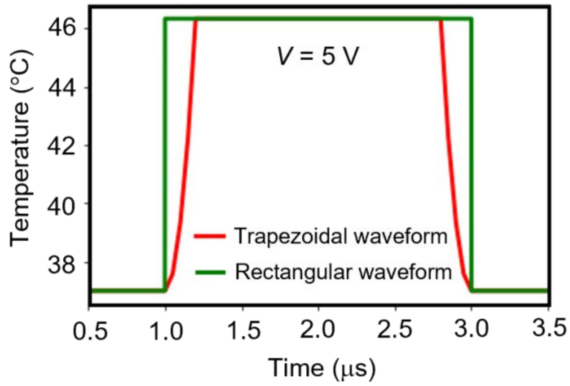

Figure S9. Thermal profiles of the WS_2/PEG-nanostructure AC-pulse model for different types of waveforms. Two different waveforms were applied to the cell-layer/nanostructure model.

References

(1) Cheng, L.; Liu, J.; Gu, X.; Gong, H.; Shi, X.; Liu, T.; Wang, C.; Wang, X.; Liu, G.; Xing, H.; Bu, W.; Sun, B.; Liu, Z. PEGylated WS_2 Nanosheets as a Multifunctional Theranostic Agent for in Vivo Dual-Modal CT/Photoacoustic Imaging Guided Photothermal Therapy. *Adv. Mater.* **2014**, *26* (12), 1886–1893. DOI: 10.1002/adma.201304497.

(2) Liu, T.; Wang, C.; Gu, X.; Gong, H.; Cheng, L.; Shi, X.; Feng, L.; Sun, B.; Liu, Z. Drug Delivery with PEGylated MoS_2 Nano-Sheets for Combined Photothermal and Chemotherapy of Cancer. *Adv. Mater.* **2014**, *26* (21), 3433–3440. DOI: 10.1002/adma.201305256.

(3) Feng, W.; Chen, L.; Qin, M.; Zhou, X.; Zhang, Q.; Miao, Y.; Qiu, K.; Zhang, Y.; He, C. Flower-like PEGylated MoS_2 Nanoflakes for near-Infrared Photothermal Cancer Therapy. *Sci. Rep.* **2015**, *5* (1), 17422. DOI: 10.1038/srep17422.

(4) Shao, J.; Xie, H.; Huang, H.; Li, Z.; Sun, Z.; Xu, Y.; Xiao, Q.; Yu, X.-F.; Zhao, Y.; Zhang, H.; Wang, H.; Chu, P. K. Biodegradable Black Phosphorus-Based Nanospheres for in Vivo Photothermal Cancer Therapy. *Nat. Commun.* **2016**, *7*, 12967. DOI: 10.1038/ncomms12967.

(5) Hu, K.; Xie, L.; Zhang, Y.; Hanyu, M.; Yang, Z.; Nagatsu, K.; Suzuki, H.; Ouyang, J.; Ji, X.; Wei, J.; Xu, H.; Farokhzad, O. C.; Liang, S. H.; Wang, L.; Tao, W.; Zhang, M.-R. Marriage of Black Phosphorus and Cu^{2+} as Effective Photothermal Agents for PET-Guided Combination Cancer Therapy. *Nat. Commun.* **2020**, *11* (1), 2778. DOI: 10.1038/s41467-020-16513-0.

(6) Hao, J.; Song, G.; Liu, T.; Yi, X.; Yang, K.; Cheng, L.; Liu, Z. In Vivo Long-Term Biodistribution, Excretion, and Toxicology of PEGylated Transition-Metal Dichalcogenides MS_2 (M = Mo, W, Ti) Nanosheets. *Adv. Sci.* **2016**, *4* (1), 1600160. DOI: 10.1002/advs.201600160.